Lifetime Prediction of DC-link Capacitors in Multiple Drives System Based on Simplified Analytical Modeling

Wang, Haoran; Huang, Shili; Kumar, Dinesh; Wang, Qian; Deng, Xiangtian ; Zhu, Guorong; Wang, Huai

Published in:
IEEE Transactions on Power Electronics

DOI (link to publication from Publisher):
10.1109/TPEL.2020.3003236

Publication date:
2021

Document Version
Accepted author manuscript, peer reviewed version

Lifetime Prediction of DC-link Capacitors in Multiple Drives System Based on Simplified Analytical Modeling

Haoran Wang, *Member, IEEE*, Shili Huang, *Student Member, IEEE*, Dinesh Kumar, *Senior Member, IEEE*, Qian Wang, *Member, IEEE*, Xiangtian Deng, *Member, IEEE*, Guorong Zhu, *Senior Member, IEEE*, Huai Wang, *Senior Member, IEEE*

***Abstract*—Lifetime prediction of DC-link capacitors in a single drive has been discussed before, which indicates that the capacitor in a standard drive meets serious reliability challenge and in slim drive does not. However, in most of the applications, drives are connected in parallel with the power grid. The large amount of harmonic distortion produced by nonlinearity drives may transmit and couple between grid and drives, which changes the stresses of devices as well as the DC-link filters. Therefore, the estimated results in single drive can not be extended to multiple drives any more. This paper investigates the lifetime of DC-link capacitors in multiple drives system. Firstly, by decoupling the interactions among grid-connected drives, a simplified equivalent circuit model and its analytical model to obtain the DC-link continuous current in multiple drives is proposed, which releases the designers from configuraing the large simulation for multiple drives. Then, applying the lifetime prediction method, the lifetime of DC-link capacitors in multiple drives are investigated, in terms of types of drives, numbers of drives and grid conditions. The results show that the lifetime of the standard drives extend in the multi-drive systems and lifetime of the slim drives decrease in the multi-drive systems, which break the previous mind. Finally, based on the proposed analytical model and lifetime estimation method, the capacitor sizing from reliability aspect for multiple slim drives are given. The outcomes of the lifetime investigation could be a guideline for the design of capacitive DC-link in multi-drive systems.**

***Index Terms*—DC-link capacitor, multi-drive systems, equivalent circuit model, lifetime**

I. Introduction

Grid-connected Adjustable Speed Drives (ASDs) with a front-end diode bridge rectifier is an effective energy saving solution for motors in various industrial, commercial, and residential applications [1], [2]. DC-link capacitors is an important part of ASDs, which serves to limit the DC-link voltage ripple, absorb harmonics, and provide a certain amount of energy storage for abnormal and transient operations [3], [4]. It contributes high percent of volume, cost and failure rate in the whole drive [5], [6].

In recent years, reliability of capacitors draws extensive attention [7–9]. The failure of these capacitors depends on both the inherent capability of the selected capacitors (e.g., rated voltage, rated current and rated lifetime) and the operational conditions (e.g., electro-thermal stresses) in the field operation [10], [11]. Depending on the structures of ASDs, different DC-link capacitors are implemented. For the standard drives with DC-link LC filter, Electrolytic Capacitors (E-caps) are commonly used due to the cost effectiveness and high energy density [12, 13, 15, 16]. However, the use of E-caps raises reliability concern. The primary cause of its failure is due to electrolyte evaporation or dielectric material degradation, which highly depends on the electro-thermal stresses [17], [18]. High ripple currents cause internal self-heating, increasing the hot-spot temperature, and resulting in aging. Moreover, it increases the Equivalent Series Resistor (ESR) over time [19], [20]. An increase in its ESR causes more heat for a given ripple current, thus increasing the hot-spot temperature rise and accelerating the degradation process. In recent years, slim DC-link drives with significantly smaller DC-link capacitance (i.e., slim drive) implemented by film capacitor (Film-cap) have been in the market [21], [22]. It benefits the reduction of harmonics and volume, and has potential to improve the reliability. Compared with the E-caps in the standard drives, Film-cap are recognized to be more reliable due to the dry plastic film served as dielectric, which achieves lower ESR and higher current capability.

The lifetime prediction and benchmarking of the capacitors in a standard drive and slim drive have been presented in literatures [23], [24]. The quantitative results are compatible with the theoretical discussion, where the slim drive shows longer lifetime than standard drive with the same loading profile [24]. However, in typical applications, drives are not working alone, which are connected in parallel with a low-voltage distribution network in a commercial or an industrial segment [25]. For example, multiple water pumps connected to a step-down transformer, multiple refrigeration and air conditioning in a automation and dairy production, numbers of drives on container ships, and so on [13], [14]. Whether the

This work was supported by the Innovation Fund Denmark through the Advanced Power Electronic Technology and Tools Project, and by project of National Natural Science Foundation of China (Grant No: 51777146 and 51977163). Partial results of this manuscript have been presented at the IEEE Energy Conversion Congress and Exposition (ECCE), 2019 sponsored by power electronics society. (*Corresponding author: Guorong Zhu.*)

Haoran Wang, Qian Wang, and Huai Wang are with the Department of Energy Technology, Aalborg University, 9220 Aalborg, Denmark (e-mail: hao@et.aau.dk, qiw@et.aau.dk, and hwa@et.aau.dk).

Shili Huang, Xiangtian Deng, and Guorong Zhu are with School of Automation, Wuhan University of Technology, China (e-mail: shili.huang@whut.edu.cn, dengxt@whut.edu.cn and zhgr_55@whut.edu.cn).

Dinesh Kumar is with Development Center, Danfoss Drives A/S, Denmark (e-mail: dineshr30@ieee.org).

This article has been accepted for publication in a future issue of this journal, but has not been fully edited. Content may change prior to final publication. Citation information: DOI 10.1109/TPEL.2020.3003236, IEEE Transactions on Power Electronics

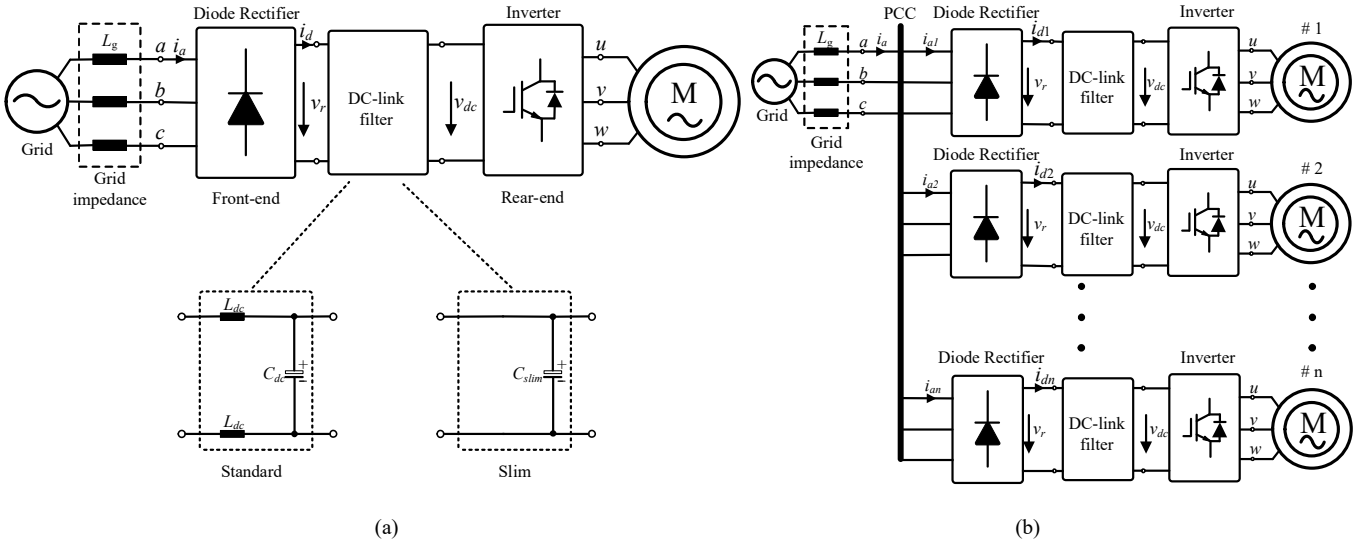

Fig. 1. Block diagram of (a) Single ASD system with standard or slim filter configuration, (b) Multi-drive systems.

reliability of DC-link capacitors in multiple drives still keep the same with that in a single drive is the industry's interest and worth to study. The existing research effort regarding to multi-drive systems mainly focus on the power quality of the grid network. The interactions between the power grid and multiple drives may introduce harmonics, which distort the grid current and voltage. Based on the simulation and experimental testing, the Total Harmonic Distortion (THD) of the grid current in multiple drives are studied [2]. However, the relationship between the reliability performance and the configurations of drives (e.g., types, numbers, and load conditions) have not been discussed before. The large amount of harmonic distortion produced by nonlinearity drives may transmit and couple between grid and multiple drives, which also changes the stress of the individual DC-link filter. Therefore, the estimated lifetime in single drive can not be extended to multiple drives. For the investigation of the lifetime of DC-link capacitors in multi-drive systems, following issues need to be addressed with:

1) DC-link current causes internal self-heating, which is a key factor of failure. For a single drive, the capacitor current can be obtained from either experimental measurements, simulations, or analytical models by using the time-domain or frequency-domain analysis [25], [26]. Nevertheless, the method cannot be simply scaled up for a system with a large number of drives due to the significantly increased complexity;

2) In a multi-drive system, the electro-thermal stresses and expected lifetime of the DC-link capacitors are altered compared to that of a single-drive system. A quantitative analysis of the impact of the number of the drives is missed in literature for optimal sizing of the capacitors in a multi-drive system.

This paper investigates the lifetime of the DC-link capacitors in multi-drive systems. It aims to find the relationship between the lifetime and the configurations of the multi-drive systems in terms of structures, numbers of drive, and grid conditions. The contributions of this paper are shown below: Firstly, an equivalent circuit model and its analytical model for multi-drive systems are proposed to derive the DC-link current of individual drive. In order to analyze the multi-drive systems with both the standard drive and slim drive in different grid conditions, the grid impedance and DC-link filters are considered in the model. To simplify the nonlinear characteristics, the heavy load operating conditions are assumed, where the DC-link current is continuous. Secondly, applying the lifetime prediction method [1], the lifetime of DC-link capacitors in multi-drive systems are investigated comprehensively from the following aspects: 1) lifetime benchmarking of DC-link capacitors in both standard drives and slim drives with scalable numbers of drives; 2) lifetime benchmarking of DC-link capacitors under different grid conditions in multi-drive systems (e.g. standard drives and slim drives); 3) lifetime evaluation of DC-link capacitors in hybrid multi-drive system. Finally, after the lifetime prediction of DC-link capacitors in various configurations and different grid conditions, the impact of the capacitor sizing on the lifetime of DC-link capacitors in multi-drive systems is studied. It serves as a guideline for proper selection of configurations of multi-drive systems and its parameters to fulfill a certain lifetime requirement.

The rest of this paper is organized as follows. In Section II, the overview of the multi-drive systems are described. In Section III, an equivalent circuit model and its analytical model for multi-drive systems to obtain the DC-link current of individual drive is presented considering AC-side and DC-side impedance. In Section IV, the lifetime prediction for different configurations of multi-drive systems under different grid conditions are investigated; The capacitor sizing criteria for multi-drive systems from the reliability aspect are discussed in Section V, followed by the conclusions in Section VI.

II. Overview of a Multi-drive Systems

The configuration of a single ASD is shown in Fig. 1 (a), where the front-end of ASD is a three-phase diode rectifier and the rear-end is consist of an inverter. Since the diode

This article has been accepted for publication in a future issue of this journal, but has not been fully edited. Content may change prior to final publication. Citation information: DOI 10.1109/TPEL.2020.3003236, IEEE Transactions on Power Electronics

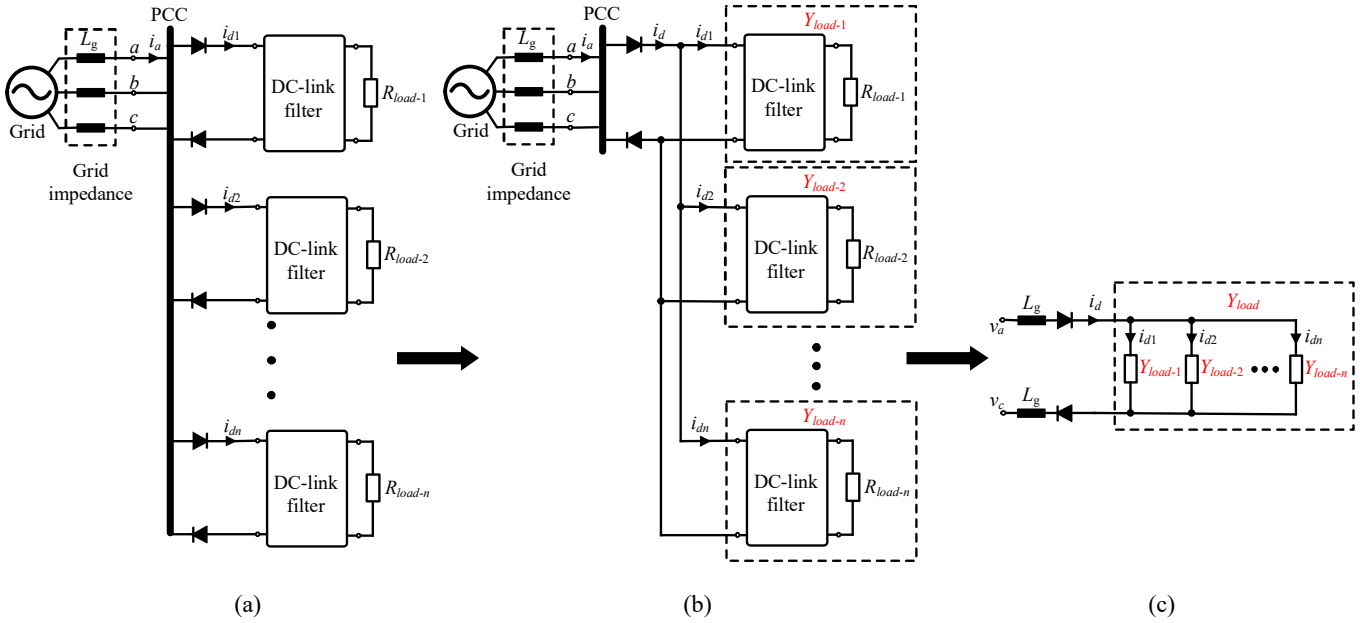

Fig. 2. Block diagram of (a) Multi-drive systems, (b) Simplified model of the multi-drive systems, (c) An equivalent circuit model of the multi-drive systems.

rectifier may cause current harmonics due to the nonlinear effects, the DC-link filter is needed to mitigate the harmonics. The widely used harmonic mitigation solution is the standard filter (i.g., LC filter), as shown in Fig. 1 (a). The standard filter is implemented with large E-caps $C_{\rm dc}$ and an inductor $L_{\rm dc}$, where the inductor is used to reduce the line harmonics emissions and the E-caps is used to reduce the fluctuation of voltage. However, the standard filter is inferior in reliability and volume aspects due to poor reliability of E-caps and the large size of inductor as well as E-caps. Another DC-link filter configuration is slim filter, as shown in Fig. 1 (a), which is implemented with a small Film-cap $C_{\rm slim}$. Slim filter is well received in the market due to its advantages in cost effectiveness and reliability aspects compared with the standard filter. But actually, in most applications, drives are connected in parallel at Point of Common Coupling (PCC) instead of single drive, as is shown in Fig. 1 (b). The configuration and parameters of multiple drives may be different and the power of individual drive is vary. The interactions between the power grid and drives will influence the equivalent impedance of the multi-drive system, which may significantly affect the electro-thermal stress of the individual DC-link capacitor, and further influence the reliability of DC-link capacitor.

This paper focuses on the reliability of DC-link capacitor in multi-drive systems, therefore, the current stress of capacitor is of great importance, which is mainly determined by the impedance of ASDs system. The impedance of single slim drive system is determined by the DC-link slim capacitor and the grid impedance, and the impedance of single standard filter is determined by the DC-link E-caps, inductor and grid impedance. The grid impedance of low-voltage distribution network is mainly determined by the size and type of step-down transformer and feeders. However, for the multiple slim or standard drives system, the grid and drives interact, which influence the impedance of individual drive. As a result, the impedance of multiple drives system as well as the reliability of DC-link capacitors depend not only on the grid impedance value and parameters of drive, but also on the configuration of the other drives connected in parallel.

III. Simplified Equivalent Circuit and Its Analytical Model

This section studies the simplified equivalent circuit model and the analytical model of multi-drive systems. Firstly, the simplified equivalent model of multi-drive system is introduced considering the interactions among drives. Then, the analytical model to acquire the DC-link capacitor current of individual drive is provided.

A. Equivalent Circuit Model

When the three-phase diode rectifier is in the conduction period, two of the input voltage sources are connected to the DC link. The interconnection impedance between drives is negligible, the multi-drive systems can be simplified in Fig. 2 (a) when the diodes are conducting. The load in the simplified equivalent mode is considered as a resistor (i.e., $R_{\rm load-k}$, k=(1,2, …, n)). Therefore, the multi-drive systems in Fig. 2 (a) can be simplified in Fig. 2 (b). The DC-link filter and the load of each drive can be modeled as a RLC or RC circuit and expressed as an admittance $Y_{\rm load-n}$. The admittance of multiple drives connected in parallel can be amalgamate into $Y_{\rm load}$ as shown in Fig. 2 (c). As a result, $Y_{\rm load}$ of equivalent circuit model is given as:

$$\begin{aligned} Y_{\rm load} &= Y_{\rm load-1} + Y_{\rm load-2} + \ldots + Y_{\rm load-n} \\ &= \frac{1}{R_{\rm load} + jX_{\rm load}} \end{aligned} \tag{1}$$

This article has been accepted for publication in a future issue of this journal, but has not been fully edited. Content may change prior to final publication. Citation information: DOI 10.1109/TPEL.2020.3003236, IEEE Transactions on Power Electronics

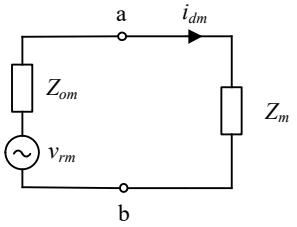

Fig. 3. Equivalent circuit for obtaining harmonic components of dc current.

For standard drives,

$$Y_{\mathrm{load-n}} = \frac{1 + j\omega C_{\mathrm{dc}} R_{\mathrm{load-n}}}{R_{\mathrm{load-n}} - \omega^2 R_{\mathrm{load-n}} L_{\mathrm{dc}} C_{\mathrm{dc}} + j\omega L_{\mathrm{dc}}} \tag{2}$$

For slim drives,

$$Y_{\mathrm{load-n}} = \frac{1 + j\omega C_{\mathrm{slim}} R_{\mathrm{load-n}}}{R_{\mathrm{load-n}}} \tag{3}$$

Based on the analysis above, the multi-drive system can be simplified by paralleling the admittance in DC-side. When the type and parameters of drives are the same, multiple admittance paralleled at DC-side can be lumped into an admittance. Then, the current of DC-link capacitor in multi-drive system can be obtained from one drive, which reduce the complexity.

B. Analytical Model

The equivalent circuit model in Fig. 2 (c) enables the analysis of multi-drive systems simpler, and it can be described in the analytical model to obtain DC-link capacitor current stress in multi-drive systems. For a balanced three-phase grid,

$$\begin{cases} v_{\mathrm{a}} = V_{\mathrm{m}} \sin\theta \\ v_{\mathrm{b}} = V_{\mathrm{m}} \sin(\theta - \frac{2\pi}{3}) \\ v_{\mathrm{c}} = V_{\mathrm{m}} \sin(\theta - \frac{4\pi}{3}) \end{cases} \tag{4}$$

where v_{a}, v_{b} and v_{c} are instantaneous value of grid phase voltage, V_{m} is the amplitude of grid phase voltage, and θ equals to ωt. The instantaneous DC-side voltage v_{r} in Fig. 1 can be expressed in terms of the voltage rectifier switching functions S_{a}, S_{b} and S_{c}.

$$v_{\mathrm{r}} = S_{\mathrm{a}} v_{\mathrm{a}} + S_{\mathrm{b}} v_{\mathrm{b}} + S_{\mathrm{c}} v_{\mathrm{c}} \tag{5}$$

Because the analysis is based on the continuous current mode, the rectifier switching function S_{a} can be expressed by the Fourier series in (6) [26]. Accordingly, S_{b} and S_{c} can be obtained by replacing θ in (6) by (θ-2π/3) and (θ-4π/3), respectively.

$$S_{\mathrm{a}} = \sum_{q=1,5,7,\ldots}^{\infty} \frac{\sqrt{3}}{\pi} \cdot \frac{(-1)^{l+1}}{q} \times \{\sin qu \cos q\theta - (1 + \cos qu) \sin q\theta\} \tag{6}$$

where q = 6l±1 (l = 0, 1, 2, …, q>0), u is an overlap angle. The overlap angle of multi-drive systems can be obtained based on the equivalent circuit model in Fig. 2 (c) [26]:

$$u = \arccos\left(1 - \frac{2\omega L_{\mathrm{g}} I_{\mathrm{d}}}{\sqrt{3} V_{\mathrm{m}}}\right) \tag{7}$$

where I_{d} is the dc component of DC-side current i_{d} in Fig. 2 (c). Substituting (4) and (6) into (5), the DC-side voltage v_{r} is given as:

$$\begin{aligned} v_{\mathrm{r}} &= V_{\mathrm{r}} + v_{\mathrm{rm}} \\ &= V_{\mathrm{r}} + \sum_{m=6,12,18,\ldots}^{\infty} (A_{\mathrm{dm}} \cos m\theta + B_{\mathrm{dm}} \sin m\theta) \end{aligned} \tag{8}$$

where

$$V_{\mathrm{r}} = \frac{3\sqrt{3} V_{\mathrm{m}}}{2\pi} \{1 + \cos u\}$$

$$A_{\mathrm{dm}} = \frac{3\sqrt{3} V_{\mathrm{m}} (-1)^p}{2\pi} \left\{ \frac{1 + \cos(m+1)u}{m+1} - \frac{1 + \cos(m-1)u}{m-1} \right\}$$

$$B_{\mathrm{dm}} = \frac{3\sqrt{3} V_{\mathrm{m}} (-1)^p}{2\pi} \left\{ \frac{\sin(m+1)u}{m+1} - \frac{\sin(m-1)u}{m-1} \right\}$$

m = 6p (p = 1, 2, 3, …)

The DC-side current i_{d} can be obtained by applying the DC-side voltage v_{r} and the impedance at the corresponding harmonics frequencies. Based on the equivalent circuit model in Fig. 2 (c), the equivalent impedance circuit for obtaining harmonic components of dc current is shown in Fig. 3. Terminals *a* and *b* connect the diode rectifier and the DC-link filter, where Z_{m} is m th impedance of the load as viewed from terminals *a* and *b* ; Z_{om} is m th impedance of the AC-side as viewed from terminals *a* and *b* and represents the grid impedance; v_{rm} is m th component of DC-side voltage v_{r}. From Fig. 2 (c), the m th impedance of the load of multiple drives system is given by:

$$Z_{\mathrm{m}} = \frac{1}{Y_{\mathrm{load}}} \tag{9}$$

The AC-side impedance Z_{om} is not equal to the grid impedance, and it is affected by the overlap angle u, Z_{om} is given by [13]:

$$Z_{\mathrm{om}} = j(2 - \frac{3u}{2\pi}) m\omega L_{\mathrm{g}} \tag{10}$$

The m th harmonic current component of DC-side current is:

$$i_{\mathrm{dm}} = \frac{v_{\mathrm{rm}}}{Z_{\mathrm{m}} + Z_{\mathrm{om}}} \tag{11}$$

Equation (8), (9), (10) and (11) give:

$$\begin{aligned} i_{\mathrm{d}} &= I_{\mathrm{d}} + \sum i_{\mathrm{dm}} \\ &= I_{\mathrm{d}} + \sum_{m=6,12,18,\ldots}^{\infty} \sqrt{2} I_{\mathrm{dm}} \cos(m\theta - \beta_{\mathrm{m}}) \end{aligned} \tag{12}$$

where

$$I_{\mathrm{d}} = \frac{V_{\mathrm{r}}}{R_{\mathrm{load}}}, I_{\mathrm{dm}} = \frac{\sqrt{(A_{\mathrm{dm}}^2 + B_{\mathrm{dm}}^2)/2}}{|Z_{\mathrm{m}} + Z_{\mathrm{om}}|}$$

$$\beta_{\mathrm{m}} = \arctan\frac{B_{\mathrm{dm}}}{A_{\mathrm{dm}}} + \arctan\frac{Im(Z_{\mathrm{m}} + Z_{\mathrm{om}})}{Re(Z_{\mathrm{m}} + Z_{\mathrm{om}})}$$

This article has been accepted for publication in a future issue of this journal, but has not been fully edited. Content may change prior to final publication. Citation information: DOI 10.1109/TPEL.2020.3003236, IEEE Transactions on Power Electronics

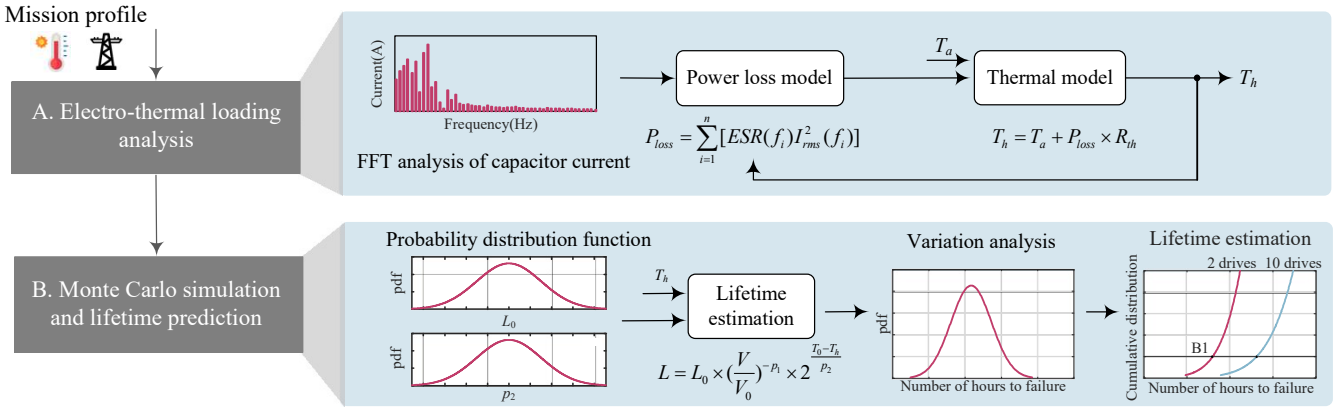

Fig. 4. Lifetime prediction procedure of DC-link capacitor. $ESR(f_{\rm i})$ is the ESR at frequency $f_{\rm i}$ and $I_{\rm rms}(f_{\rm i})$ is the Root Mean Square (RMS) value of the harmonic current at frequency $f_{\rm i}$. $T_{\rm h}$ is the hot-spot temperature and $T_{\rm a}$ is the ambient temperature, which is 60 °C in this study. $R_{\rm th}$ is the thermal resistance of capacitor between the hot-spot and ambient. L_0 is the rated lifetime at rated voltage V_0 and temperature T_0. V is the voltage under operation condition. p_1 is in the range of 7 to 9.4 for Film-caps, and 3 to 5 for E-caps based on the existing lifetime model [3]. p_2 is a coefficient assumed to be 10.

TABLE I
SPECIFICATION OF THE ASDS SYSTEM AND THE DC-LINK CAPACITOR CONFIGURATION OF COMMERCIAL PRODUCT.

ASDs system specification		Standard LC filter (C_{dc})		Slim capacitor filter (C_{slim})
Rated power (kW)	7.5	Physical configurations	Four 450V/680μF electrolytic capacitor	1100V/30μF Film capacitor
Grid frequency (Hz)	50	Part number	TDK. B43644A5687M	TDK. B32778G0306
Grid phase RMS voltage (V)	230	ESR of single capacitor	140 mΩ @100Hz	14 mΩ @100Hz
DC-link voltage (V)@7.5kW balanced grid voltage	535	Thermal resistance (R_{th})	6 °C/W	13 °C/W
Grid impedance (L_g)(soft)	130μH	Rated load lifetime	5000 hours @105 °C and rated ripple current	100000 hours @70 °C and rated ripple current
Grid impedance (L_g) (stiff)	2μH	L_{dc}	1.25 mH	

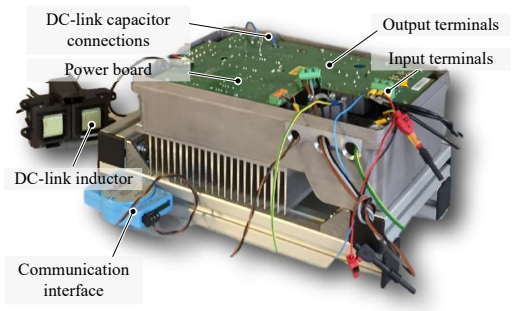

Fig. 5. Experimental prototype of the motor drive with DC-link filter.

The obtained current $i_{\rm d}$ in (12) is the DC-side current of equivalent circuit of multi-drive systems. Therefore, the dc current of drive n is:

$$\begin{aligned} i_{\rm dn} &= I_{\rm dn} + \sum i_{\rm dn-m} \\ &= i_{\rm d} \frac{Y_{\rm load-n}}{Y_{\rm load}} \end{aligned} \tag{13}$$

where $I_{\rm dn}$ is the dc component of DC-side current of drive n. The DC-link capacitor current of individual drive can be obtained from the DC-side current $i_{\rm dn}$. By analyzing the characteristics of current shunt, we can get that the harmonic of DC-side current $i_{\rm dn}$ are absorbed by DC-link capacitor. Therefore, the DC-link capacitor current equals to the harmonic of DC-side current, which equals to $\sum i_{\rm dn-m}$.

IV. LIFETIME PREDICTION OF DC-LINK CAPACITORS IN MULTI-DRIVE SYSTEMS

This section studies the lifetime prediction of DC-link capacitors in multi-drive systems. Firstly, the lifetime prediction method with the proposed capacitor current analytical model is validated step by step. Then, the impact of drives number and the grid conditions on the DC-link capacitor lifetime are investigated. In order to see the impact from different numbers more clearly, the impact from other factors (such as the detail parameters and operating conditions of individual drive) are minimized. Therefore, the operating conditions are assumed the same and loads are the same resistors, which can be changed for different applications.

A. Lifetime Prediction Method of DC-link Capacitors

The lifetime prediction procedure of DC-link capacitor is shown in Fig. 4, which is divided into two parts. The first part is the electro-thermal loading analysis, which aims to estimate the hot-spot temperature by using the current stress of capacitor from different loading conditions. The obtained hot-spot temperature serves as the input of the second part, which is Monte Carlo simulation and lifetime prediction considering the parameters variation in the lifetime model.

This article has been accepted for publication in a future issue of this journal, but has not been fully edited. Content may change prior to final publication. Citation information: DOI 10.1109/TPEL.2020.3003236, IEEE Transactions on Power Electronics

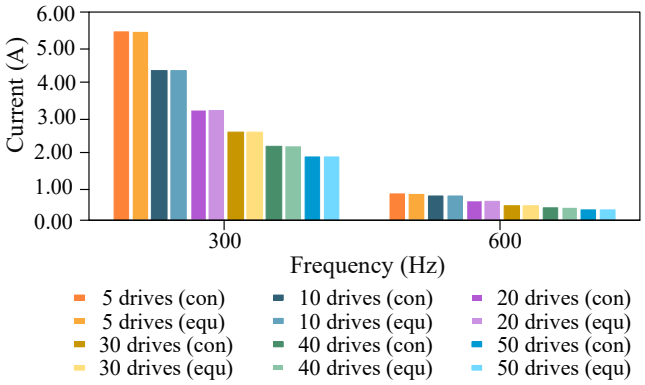

Fig. 6. Comparison between the DC-link capacitor current obtained by conventional model and equivalent circuit model in standard drives system under soft grid condition (L_g= 130 μH).

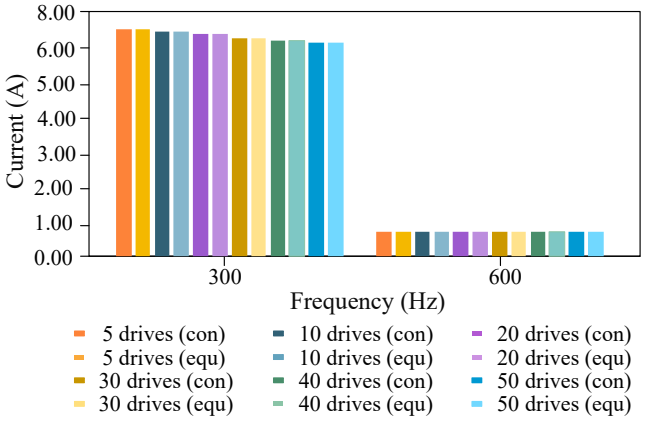

Fig. 7. Comparison between the DC-link capacitor current obtained by conventional model and equivalent circuit model in standard drives system under stiff grid condition (L_g= 2 μH).

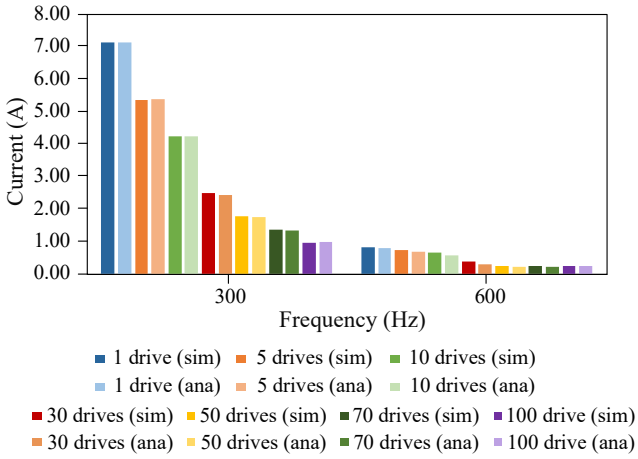

Fig. 8. Comparison between the DC-link capacitor current obtained by simulation and analytical model in standard drives system under soft grid condition (L_g= 130 μH).

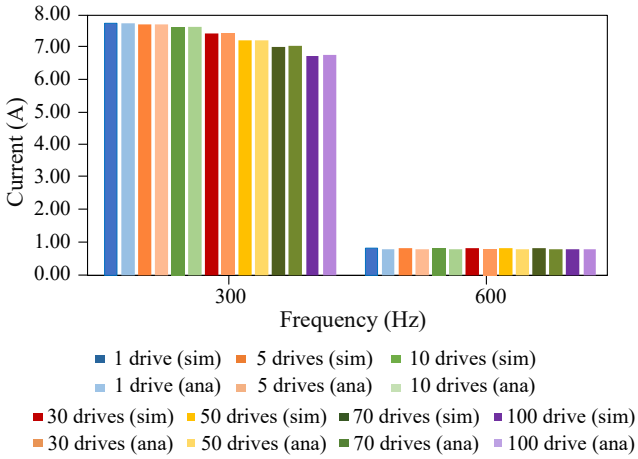

Fig. 9. Comparison between the DC-link capacitor current obtained by simulation and analytical model in standard drives system under stiff grid condition (L_g= 2 μH).

The experiment prototype of motor drive is shown in Fig. 5 and the specification of ASDs system is shown in Table I. The values of ASDs system specification in Table I are based on commercial products and a real industrial condition, where the values of standard LC filter and slim capacitor filter are calculated according to cut-off frequency. Due to the heat dissipation from the diode bridge, DC-link filter, and inverter, the local temperature in the enclosure is defined as 40-60 °C instead of the room temperature. The validation of equivalent circuit model is implemented in standard drives system with both soft (i.e. the grid impedance is 130 μH) and stiff (i.e. the grid impedance is 2 μH) grid conditions. The results are shown in Fig. 6 and Fig. 7, respectively. It shows that the capacitor current stress obtained by equivalent circuit model is almost the same with that in the conventional model with numbers of ASDs. The analytical model studied in Section III-B is also validated in standard drives system with soft and stiff grid conditions, and the results are shown in Fig. 8 and Fig. 9, respectively. It shows that the DC-link capacitor current obtained by the proposed analytical model agrees well with that obtained by simulation and the absolute value of difference between is less then 0.1A. It should be noted that the analytical model applied in this paper is suitable for continuous current mode only, which is important for lifetime prediction as heavy load condition will contribute to higher current stress to DC-link capacitor.

The hot-spot temperature of the DC-capacitor can be estimated based on its ESR and the harmonic current. ESR is frequency dependent. For example, the ESR of E-caps decreases with the higher frequency, which is shown in Fig. 10, however, it is applicable for a certain frequency range, after that, ESR is increasing due to skin effect.

The hot-spot temperature is given as [1]:

$$T_{\mathrm{h}} = T_{\mathrm{a}} + \sum_{i=1}^{n} R_{\mathrm{th}} \times [ESR(f_{\mathrm{i}}) \times I^2_{\mathrm{rms}}(f_{\mathrm{i}})] \qquad (14)$$

where T_{h} is the hot-spot temperature and T_{a} is the ambient temperature, which is 60 °C in this study. R_{th} is the thermal resistance of capacitor between the hot-spot and ambient, and the value of it is shown in Table I. $ESR(f_{\mathrm{i}})$ is the ESR at frequency f_{i} and $I_{\mathrm{rms}}(f_{\mathrm{i}})$ is the Root Mean Square (RMS)

This article has been accepted for publication in a future issue of this journal, but has not been fully edited. Content may change prior to final publication. Citation information: DOI 10.1109/TPEL.2020.3003236, IEEE Transactions on Power Electronics

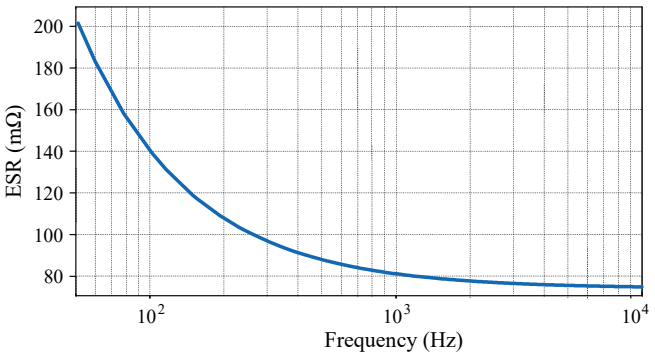

Fig. 10. ESR characteristic curve of E-caps with part number: TDK. B43644A5687M.

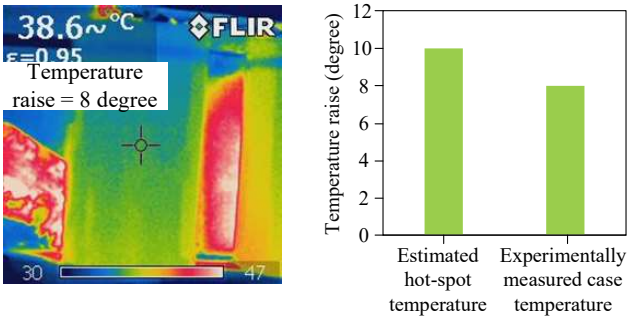

Fig. 11. (a) Tested case temperature in standard filter under soft grid condition, (b) Comparison between experimental and estimated capacitor temperature in standard filter under soft grid condition.

value of the harmonic current at frequency f_{i}. The hot-spot temperature of DC-link capacitor is estimated to be 70 °C based on the thermal model, the ESR characteristic of E-caps and the capacitor current. The experimentally measured case temperature in standard filter under soft grid condition is shown in Fig. 11 (a), and the comparison between experimental and estimated temperature is shown in Fig. 11 (b). The case temperature of capacitors is measured because the capacitors in testing setup do not have temperature sensors inside. The difference between the estimated and experimental temperature is about 2 degree in Fig. 11 (b).

The lifetime prediction model used in this paper is given as[1]:

$$L = L_0 \times (\frac{V}{V_0})^{-p_1} \times 2^{\frac{T_0 - T_{\mathrm{h}}}{p_2}} \tag{15}$$

where L_0 is the rated lifetime at rated voltage V_0 and temperature T_0. V and T_{h} are the voltage and hot-spot temperature under operation condition. p_1 is 7 to 9.4 for Film-cap, and 3 to 5 for E-caps. p_2 is a coefficient assumed to be 10 [3].

Two types of parameter variations are considered in Monte Carlo simulation: a) parameter variations in the applied lifetime prediction model; b) parameter variations due to the difference of manufacturing process among capacitors with the same part number. For the first type of variation, each lifetime prediction model has its limitations owing to the test conditions, component manufacturing process and failure mechanism are specific. Therefore, the variation of p_2 is taken into account. For the second type of variation, the variation of L_0 and T_{h} are taken into account because it has a direct effect on the lifetime of capacitor. All parameters experience 5% variation with a certain confidence level (e.g., 90%) [1] by means of normal probability distribution functions as shown in Fig. 12.

B. Lifetime Prediction of DC-link Capacitors with Scalable Number of Drives

In typical applications, drives are connected in parallel at PCC (Point of Common Coupling). The interactions between the power grid and multiple drives may influence the electro-thermal stress of the individual DC-link capacitor, which will further influence the reliability of DC-link capacitor. Therefore, the relationship between the reliability of DC-link capacitor and the number of drives is studied in this paper.

The lifetime prediction of DC-link capacitor in two types of DC-link configuration are considered, which are standard *LC* filter and slim capacitor filter. Although the rated power of ASDs is 7.5kW, the drives operate at partial load conditions in most application. As a result, ASDs system is considered to operate at 5kW in this paper. It should be noted that the higher rated power of ASDs will contribute to larger current stress of DC-link capacitor and finally reduce the DC-link capacitor lifetime. The electrical stress of DC-link capacitor is highly affected by the impedance of ASDs, so the impedance characteristics is of great importance. According to Fig. 2 (c) and (1), the impedance of multiple standard or slim drives system can be acquired as n (the number of ASDs connected in parallel) times of that in single ASD:

$$Z_{\mathrm{n}} = \frac{1}{nY_{\mathrm{load-n}}} + 2j\omega L_{\mathrm{g}} \tag{16}$$

The impedance characteristics of multiple standard and slim ASDs are shown in Fig. 13 (a) and (b), respectively. It can be seen that: a) for multiple standard drives system, the impedance at 300 Hz becomes larger with more drives connected in parallel, which will result in the current of DC-link capacitor decreases with more standard drives connected in parallel; b) for multiple slim drives system, the impedance at 300 Hz decreases first and then increases, when the number of drives increases from 1 to 100, so as to the current stress of dc-link capacitor increases first and then decrease; c) the impedance of single slim ASD system at 1800 Hz is the lowest, which will result in the current of DC-link capacitor in single slim ASD is the largest at 1800 Hz; d) the impedance of 5 slim ASDs system at 900 Hz is the lowest, which will result in the current of DC-link capacitor in 5 slim ASDs is the largest at 900 Hz; e) the impedance of 10 slim ASDs system at 600 Hz is the lowest, which will result in the current of DC-link capacitor in 10 slim ASDs is the largest at 600 Hz; f) the impedance of 30 slim ASDs system at 300 Hz is the lowest, which will result in the current of DC-link capacitor in 30 slim ASDs is the largest at 300 Hz.

The DC-link capacitor current spectrum of scalable standard and slim drives under soft grid condition are shown in Fig.

This article has been accepted for publication in a future issue of this journal, but has not been fully edited. Content may change prior to final publication. Citation information: DOI 10.1109/TPEL.2020.3003236, IEEE Transactions on Power Electronics

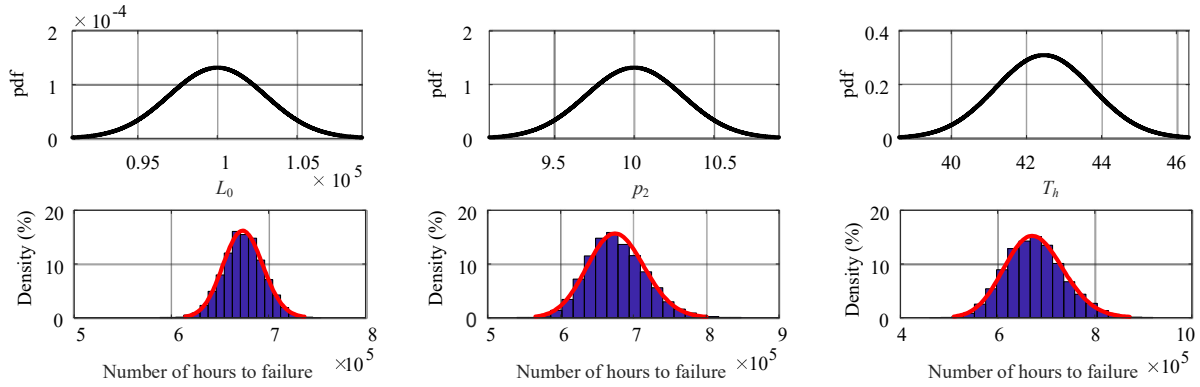

Fig. 12. Probability density functions of the parameters under analysis and lifetime probability distribution function.

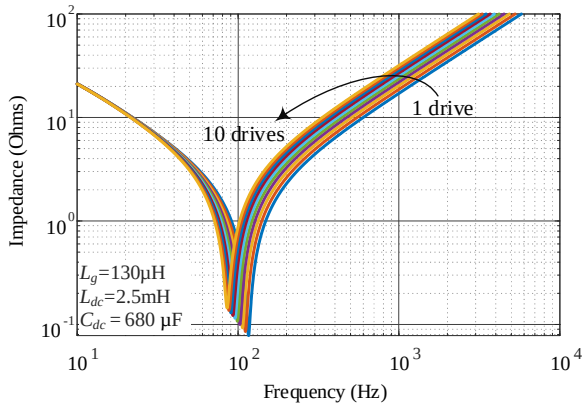

(a) Impedance characteristics of multiple standard ASDs

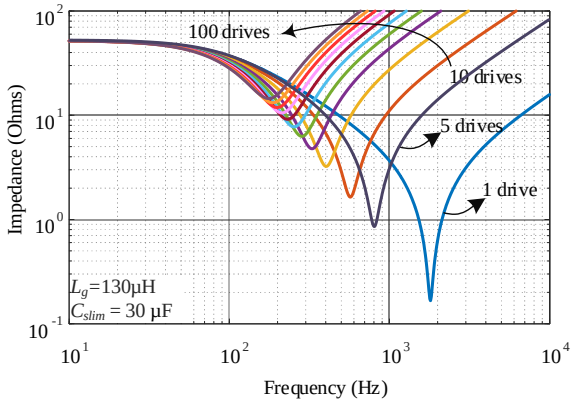

(b) Impedance characteristics of multiple slim ASDs

Fig. 13. Impedance characteristics of multiple ASDs system under soft grid condition (L_g= 130 μH).

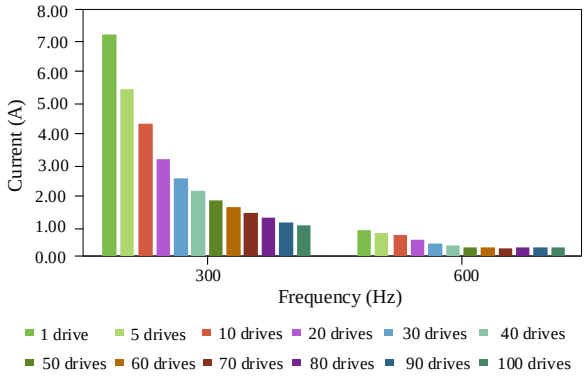

(a) DC-link capacitor current spectrum of scalable standard drives under soft grid conditions

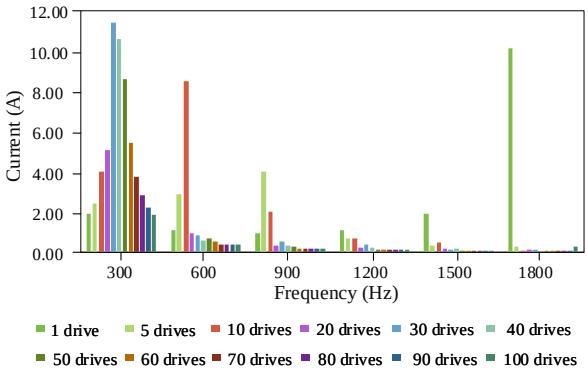

(b) DC-link capacitor current spectrum of scalable slim drives under soft grid conditions

Fig. 14. DC-link capacitor current spectrum with scalable numbers of drives.

14 (a) and (b), respectively. It can be seen from the current spectrum that: a) with more standard drives connected in parallel, the current of DC-link capacitor decreases, which is due to the impedance of multiple standard drive increases with the number of standard drive increases; b) with more slim drives connected in parallel, the current component of DC-link capacitor mainly appears at 300 Hz; c) the largest current component in 1, 5, 10 and 30 slim drives appears at 1800 Hz, 900 Hz, 600 Hz and 300 Hz, respectively, the reason for the large current component is the resonant frequency of 1, 5, 10 and 30 slim drives are close to 1800 Hz, 900 Hz, 600 Hz and 300 Hz, respectively; The obtained DC-link capacitor current spectrum is accordance with impedance characteristics analysis.

The estimated lifetime of DC-link capacitor in multiple standard and slim ASDs under soft grid condition are shown in Fig. 15 (a) and (b), respectively. It can be obtained that: a) considering the number of standard drives increases from 1 to 100, the B1 lifetime of DC-link capacitor extended from

This article has been accepted for publication in a future issue of this journal, but has not been fully edited. Content may change prior to final publication. Citation information: DOI 10.1109/TPEL.2020.3003236, IEEE Transactions on Power Electronics

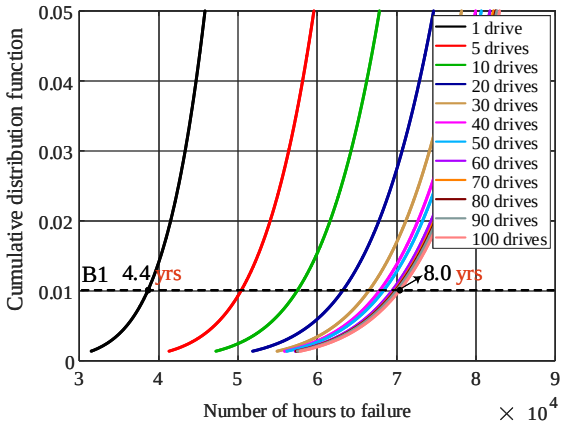

(a) Lifetime estimation of DC-link capacitor in multiple standard ASDs under soft grid conditions

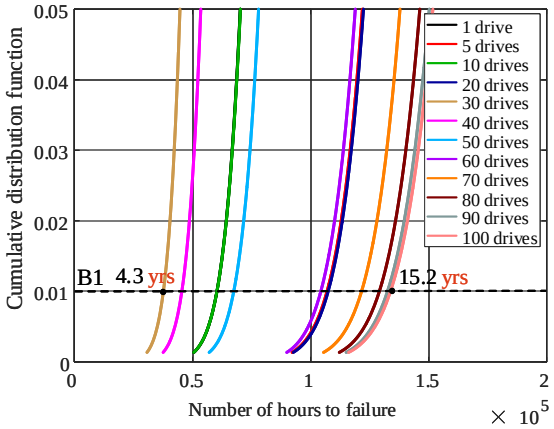

(b) Lifetime estimation of DC-link capacitor in multiple slim ASDs under soft grid conditions

Fig. 15. Lifetime estimation of DC-link capacitor in multiple standard and slim ASDs under soft grid condition (L_g= 130 μH).

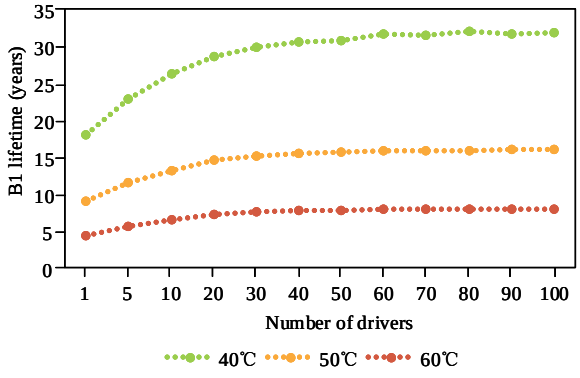

(a) B1 lifetime of DC-link capacitor in multiple standard drives under soft grid and scalable ambient temperature

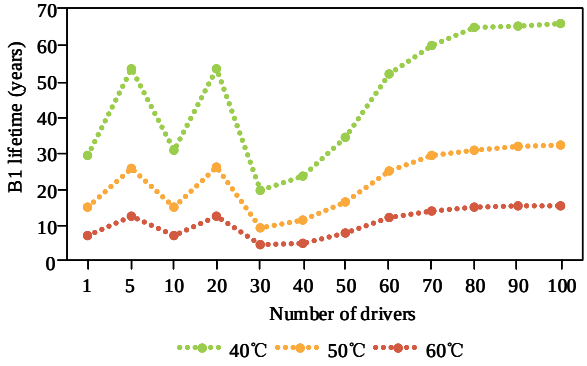

(b) B1 lifetime of DC-link capacitor in multiple slim drives under soft grid and scalable ambient temperature

Fig. 16. B1 lifetime of multiple drives system versus drive numbers with different ambient temperature.

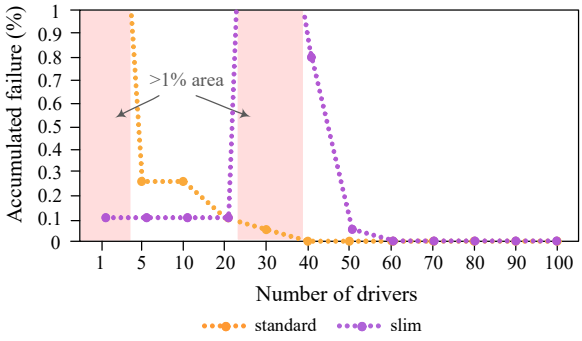

Fig. 17. Accumulated failure at 5 years lifetime of multiple drives system versus drive numbers.

4.4 years to 8.0 years; b) the shortest B1 lifetime of multiple slim ASDs is 4.3 years and appears at 30 slim drives, which is due to the current of DC-link capacitor in 30 slim drives system at 300 Hz is the largest. In order to analyze the influence of drive numbers on the DC-link capacitor lifetime more intuitively, the B1 lifetime versus drive numbers curve is shown in Fig. 16 (a) and (b), in which different ambient temperature is considered, it can be seen that: a) the B1 lifetime of multiple ASDs at same configurations becomes lower with higher ambient temperature, and the tendency of capacitor B1 lifetime with drives number are the same at different ambient temperature; b) the B1 lifetime of multiple slim ASDs changes regularly when the number of drives is greater than 30, and the B1 lifetime of 10 slim drives is relatively small, that is due to the impedance of 10 slim drives in 600 Hz is the smallest. The accumulated failure at 5 years lifetime of multiple drives system is shown in Fig. 17, it can be seen that: a) the accumulated failure at 5 years lifetime of standard drives decreases with the increase of drives number, and the accumulated failure at 5 years lifetime of one standard drive is higher than 1%; b) the accumulated failure at 5 years lifetime of slim drives is less than 1% except 30 and 40 drives systems.

C. Lifetime Prediction of DC-link Capacitors with Scalable Grid Conditions

The reliability of DC-link capacitor in multiple drives is mainly determined by the impedance of ASDs system, and the grid condition is one of the factors that influence the system impedance. Therefore, the impact of grid conditions on the

This article has been accepted for publication in a future issue of this journal, but has not been fully edited. Content may change prior to final publication. Citation information: DOI 10.1109/TPEL.2020.3003236, IEEE Transactions on Power Electronics

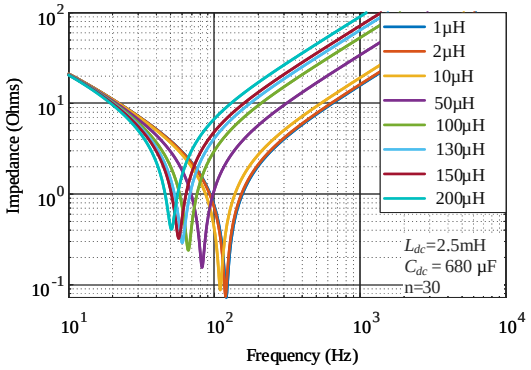

(a) Impedance characteristics of 30 standard ASDs under scalable grid conditions

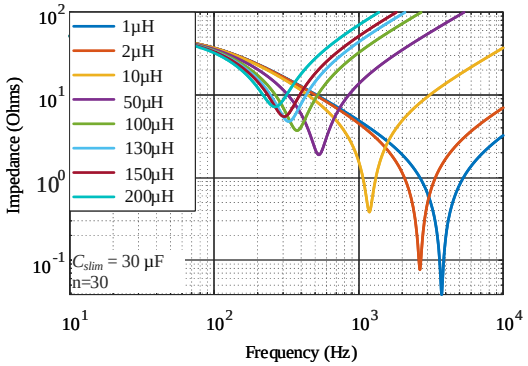

(b) Impedance characteristics of 30 slim ASDs under scalable grid conditions

Fig. 18. Impedance characteristics of multiple ASDs system under scalable grid conditions.

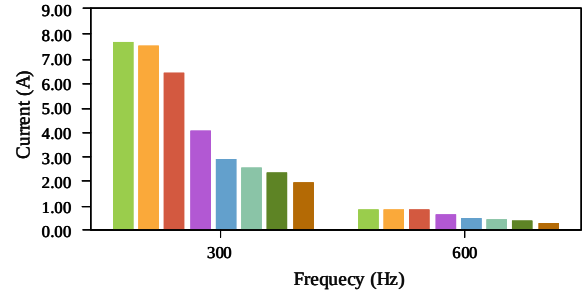

(a) DC-link capacitor current spectrum of 30 standard drives under scalable grid conditions

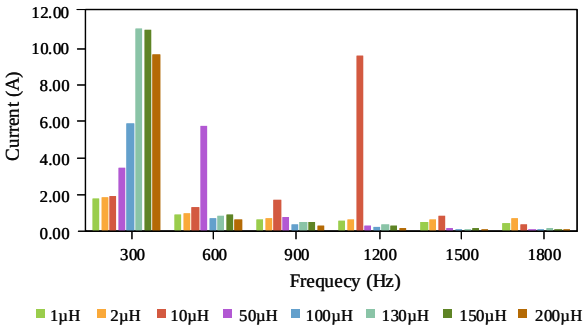

(b) DC-link capacitor current spectrum of 30 slim drives under scalable grid conditions

Fig. 19. DC-link capacitor current spectrum under scalable grid conditions.

reliability of multiple drives system is studied in this section. The results in Section IV-B show that the reliability of 30 slim drives is the lowest, therefore, the reliability of DC-link capacitor in 30 standard and slim drives with scalable grid conditions is studied in this section.

The impedance characteristics of 30 standard and slim ASDs under scalable grid conditions are shown in Fig. 18 (a) and (b), respectively. It can bee seen that: a) with the grid impedance increases from 1 μH to 200 μH, the impedance of 30 standard ASDs increases when the frequency is greater than 200 Hz, which will result in the current of DC-link capacitor in 30 standard drives system decreases with the grid impedance increases; b) when the grid impedance is 10 μH, the impedance of 30 slim ASDs at 900 Hz and 1200 Hz is the smallest, which will result in the largest DC-link capacitor current component at 900 Hz and 1200 Hz; c) when the grid impedance is 50 μH, the impedance of 30 slim ASDs at 600 Hz is the smallest, which will result in the largest DC-link capacitor current component at 600 Hz; d) when the grid impedance is 130 μH and 150 μH, the impedance of 30 slim ASDs at 300 Hz is the smallest, which will result in the largest DC-link capacitor current component at 300 Hz.

The DC-link capacitor current spectrum of 30 standard and slim ASDs under scalable grid conditions are shown in Fig. 19 (a) and (b), respectively. It can be seen from the current spectrum that: a) with the grid impedance increases from 1 μH to 200 μH, the current of DC-link capacitor in 30 standard ASDs decreases; b) the current of DC-link capacitor in 30 slim ASDs mainly appears at 300 Hz, and the largest current component at 300 Hz, 600 Hz, 900 Hz and 1200 Hz are accordance with the analysis in impedance characteristics.

The estimated lifetime of DC-link capacitor in 30 standard and slim ASDs under scalable grid conditions are shown in Fig. 20 (a) and (b), respectively. It can be obtained that: a) with the grid impedance increases from 1 μH to 200 μH, the B1 lifetime of DC-link capacitor in 30 standard ASDs extended from 4.0 years to 7.8 years, which is due to the electro-thermal stress of 30 standard drives system decreases with the grid impedance increases; b) the shortest B1 lifetime of 30 slim ASDs appear at 130 μH and 150 μH grid configurations (i.e., 4.3 years), which is due to the electro-thermal stress of 30 slim ASDs with 130 μH and 150 μH grid configurations are the largest; c) the longest B1 lifetime appears at 1 μH grid configuration (i.e., 15.2years), which is due to the electro-thermal stress of 30 slim ASDs with 1 μH grid configuration is the smallest. The B1 lifetime versus grid impedance curve is shown in Fig. 21, it can be seen that: a) the B1 lifetime of capacitor in 30 standard ASDs extend when the grid impedance becomes larger; b) with the grid impedance increases from 1 μH to 200 μH, the B1 lifetime of capacitor in 30 slim ASDs fluctuates, which is determined by the ASDs impedance characteristics; c) the B1 lifetime in 30 slim ASDs is longer than that of in 30 standard standard ASDs when the grid impedance is less than 100 μH. The accumulated failure at 5 years lifetime of multiple drives system is shown in Fig. 22, it can be seen that: a) the accumulated failure at 5 years lifetime of 30 standard drives decreases with the increase of

This article has been accepted for publication in a future issue of this journal, but has not been fully edited. Content may change prior to final publication. Citation information: DOI 10.1109/TPEL.2020.3003236, IEEE Transactions on Power Electronics

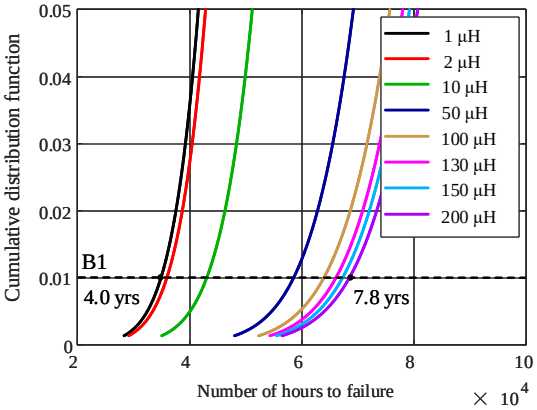

(a) Lifetime estimation of DC-link capacitor in 30 standard ASDs under scalable grid conditions

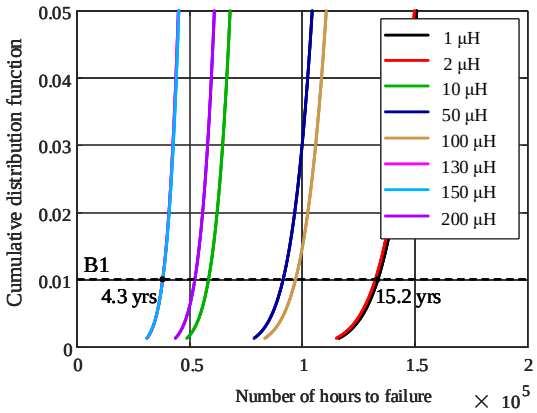

(b) Lifetime estimation of DC-link capacitor in 30 slim ASDs under scalable grid conditions

Fig. 20. Lifetime estimation of DC-link capacitor in 30 standard and slim ASDs under scalable grid conditions.

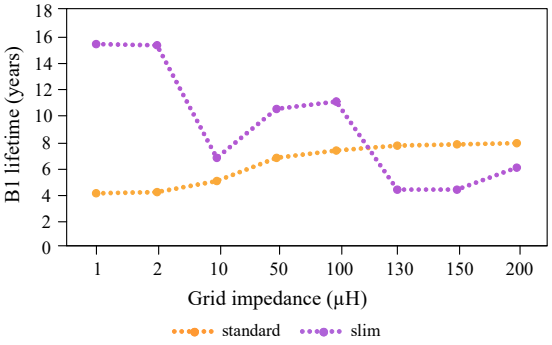

Fig. 21. B1 lifetime of 30 drives system versus grid impedance.

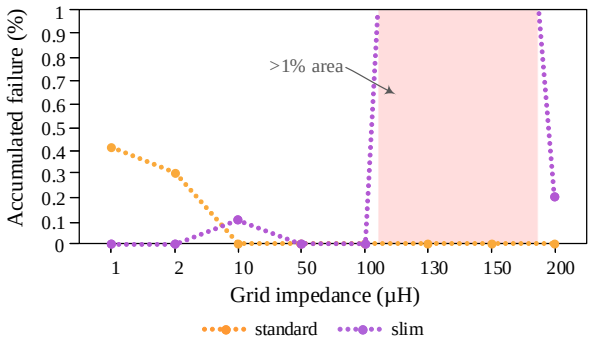

Fig. 22. Accumulated failure at 5 years lifetime of 30 drives system versus grid impedance.

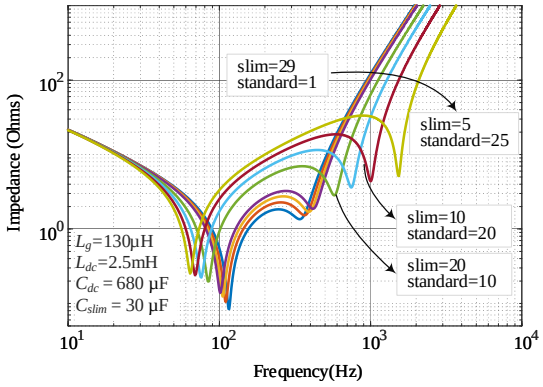

(a) Impedance characteristics of standard drives in hybrid ASDs

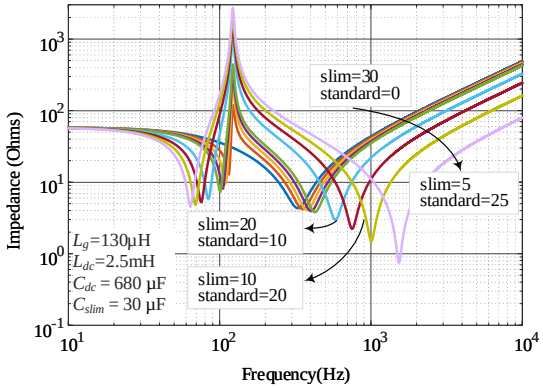

(b) Impedance characteristics of slim drives in hybrid ASDs

Fig. 23. Impedance characteristics of standard drive and slim drive in hybrid ASDs system under soft grid conditions. Keep the total number of drive to 30 and increase the percentage of standard drive.

grid impedance; b) the accumulated failure at 5 years lifetime of 30 slim drives is less than 1% except in 130 μH and 150 μH grid configurations.

D. Lifetime Prediction of DC-link Capacitors in Hybrid ASDs System

This section studies the lifetime of dc-link capacitors in hybrid ASDs system with multiple standard and slim drives. From the above section, it can be seen that the DC-link capacitor in 30 slim drives under soft grid has worse reliability compared with other numbers of slim drives, which is mainly due to the resonant frequency of 30 slim drives system is close to 300 Hz. As a further research, the hybrid drives system studied in this section focus on two scenarios: a) keep the total number of drives unchanged (e.g. 30) and increase the number of standard drive; b) keep the number of slim drives unchanged (e.g. 30) and increase the number of standard drive.

1) Constant Total Number of Hybrid Drives: In this section, the total number of hybrid drives is kept constant, while the hybrid percentage of standard and slim drives varies. The

This article has been accepted for publication in a future issue of this journal, but has not been fully edited. Content may change prior to final publication. Citation information: DOI 10.1109/TPEL.2020.3003236, IEEE Transactions on Power Electronics

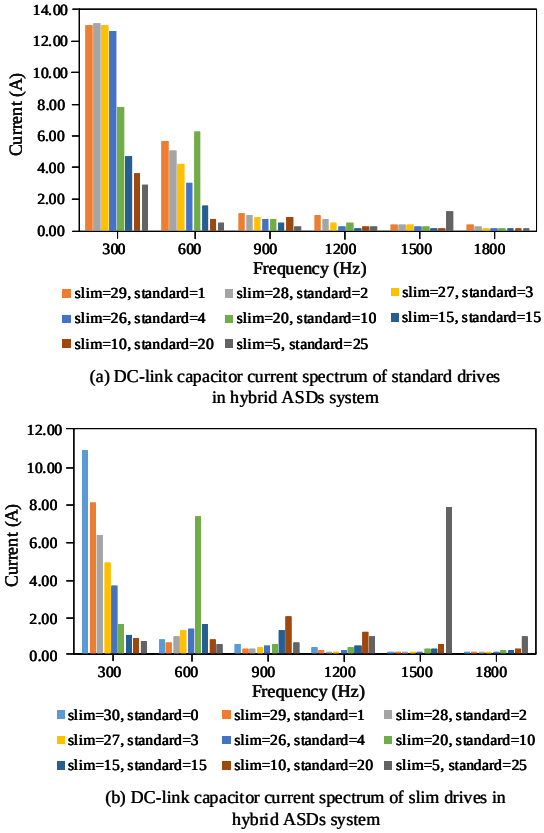

Fig. 24. DC-link capacitor current spectrum of standard drive and slim drive in hybrid ASDs system under soft grid conditions. Keep the total number of drive to 30 and increase the percentage of standard drive.

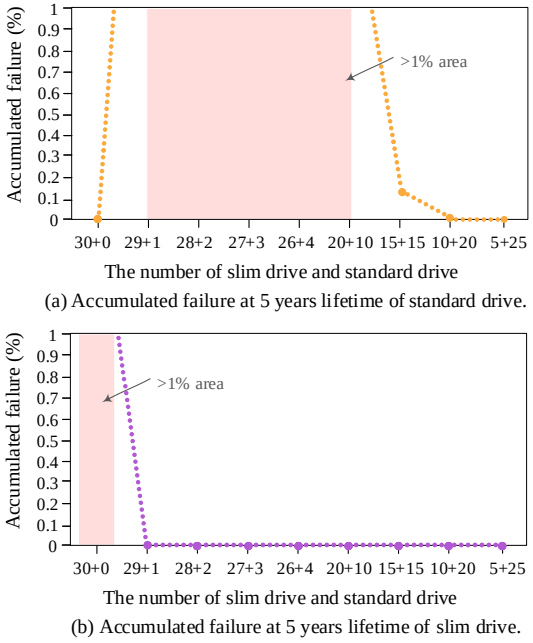

Fig. 25. Accumulated failure at 5 years lifetime of hybrid ASDs system under soft grid conditions. Keep the total number of drive to 30 and increase the percentage of standard drive.

impedance characteristics of standard drive and slim drive in hybrid ASDs system under soft grid conditions are shown in Fig. 23 (a) and (b), respectively, in which the total number of drives is kept to 30. It can bee seen that: a) with the number of standard drive increases from 1 to 25, one resonant frequency reduces from 100 Hz to 60 Hz, while the other one increase from 300 Hz to 1000 Hz; b) the resonant frequency of standard drive and slim drive in the combination of 20 slim drives and 10 standard drives system is close to 600 Hz, which will result in high DC-link capacitor current at 600 Hz; similarly, the resonant frequency of standard drive and slim drive in the combination of 10 slim drives and 20 standard drives system is close to 900 Hz, which results in high DC-link capacitor current at 900 Hz;

The DC-link capacitor current spectrum of standard drive and slim drive in hybrid ASDs system under soft grid conditions are shown in Fig. 24 (a) and (b), respectively. It can be seen from the current spectrum that: a) the current of DC-link capacitor in standard drive and slim drive mainly appears at 300 Hz and 600 Hz; b) the current component at 600 Hz is the largest when there are 20 slim drives and 10 standard drives, which is due to its resonant frequency is close to 600 Hz; c) similarly, the maximum current component at 900 Hz, 1200 Hz, 1500 Hz and 1800 Hz can be explained in the same way.

The accumulated failure at 5 years for standard drive and slim drive in hybrid ASDs system under soft grid conditions are shown in Fig. 25 (a) and (b), respectively. it can be seen that: a) the accumulated failure at 5 years for standard drives is less than 1% when the number of standard drive is greater than 15; b) the accumulated failure at 5 years for slim drives is less than 1% when standard drive is added; c) when the total number of drives is kept to 30 and increase the number of standard drive, the reliability of slim drive is improved, however, the standard drive have higher reliability only when the number of standard drives reaches to 15.

2) Constant Number of Slim Drives: In this section, the number of slim drives keeps constant and the total number increases by adding multiple standard drives. The impedance characteristics of standard drive and slim drive in hybrid ASDs system under soft grid conditions are shown in Fig. 26 (a) and (b), respectively. It can be seen that: a) with the number of standard drive increases from 1 to 30, one resonant frequency of standard drive increases from 300 Hz to 800 Hz, while the other one reduces from 100 Hz to 60 Hz; b) the resonant frequency of standard drive and slim drive in the combination of 30 slim drives and 25 standard drives system is close to 600 Hz, which results in high DC-link capacitor current at 600 Hz;

The DC-link capacitor current spectrum of standard and slim hybrid ASDs system under soft grid conditions are shown in Fig. 27 (a) and (b), respectively. It can be seen from the current spectrum that: a) the current of DC-link capacitor in standard drive and slim drive mainly appears at 300 Hz and 600 Hz; b) the current component at 600 Hz is the largest when the number of drives is the combination of 30 slim drives and 25 standard drives, which is due to its resonant frequency is close to 600 Hz; c) similarly, the maximum current component at 900 Hz, 1200 Hz, 1500 Hz and 1800 Hz can be explained

This article has been accepted for publication in a future issue of this journal, but has not been fully edited. Content may change prior to final publication. Citation information: DOI 10.1109/TPEL.2020.3003236, IEEE Transactions on Power Electronics

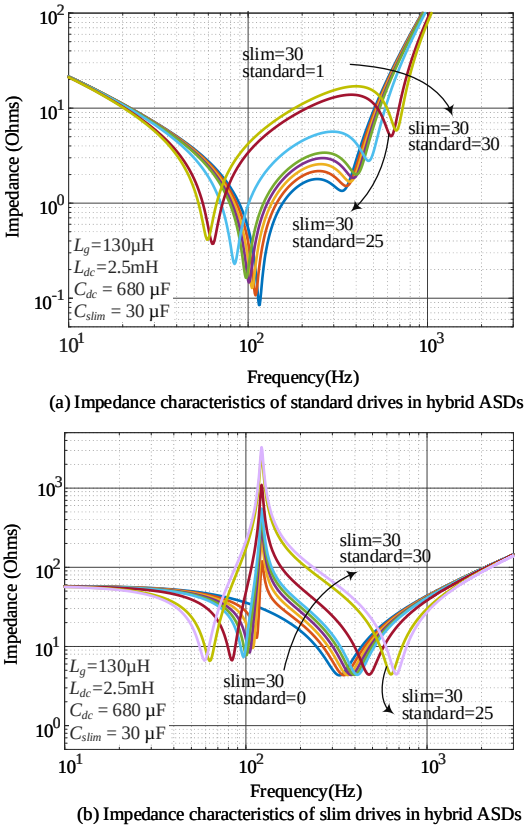

Fig. 26. Impedance characteristics of standard drive and slim drive in hybrid ASDs system under soft grid conditions. Keep the number of slim drive to 30 and increase the number of standard drive.

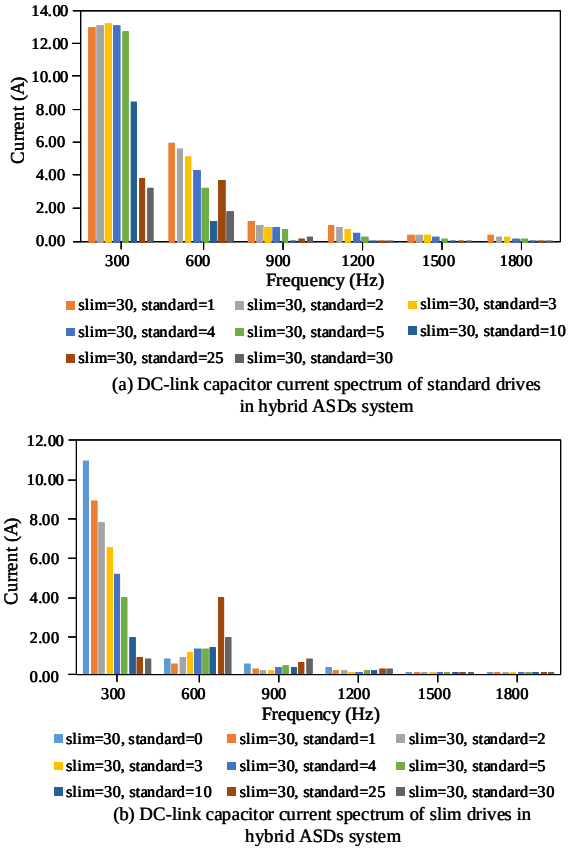

Fig. 27. DC-link capacitor current spectrum of standard drive and slim drive in hybrid ASDs system under soft grid conditions. Keep the number of slim drive to 30 and increase the number of standard drive.

in the same way.

The accumulated failure at 5 years for standard drive and slim drive in hybrid ASDs system under soft grid conditions are shown in Fig. 28 (a) and (b), respectively, in which the number of slim drive is kept to 30. it can be seen that: a) the accumulated failure at 5 years lifetime of standard drives is less than 1% when the number of standard drives is greater than 25; b) the accumulated failure at 5 years lifetime of slim drives is less than 1% when standard drives is added; c) when the number of slim drive is kept to 30 and increase the number of standard drives, the reliability of slim drives is improved, however, the standard drives have higher reliability only when the number of standard drives reaches to 25.

The results of two types of hybrid ASDs systems show that: comparing with 30 slim drives system, the slim drives in hybrid ASDs system studied in this section have higher reliability, however, the standard drive meet relability issue when the number is less than 10.

V. Capacitor Sizing of Multi-drive Systems Considering Reliability Performance

Section IV investigates the reliability of DC-link capacitor in multiple standard and slim ASDs system, and the results show that the reliability of DC-link capacitor in multiple slim drives is sensitive to the capacitance of the DC-link capacitor in the scalable numbers of drives and grid impedance. The capacitor sizing for single ASD from the aspect of power quality has been studied before, however, the study in multiple slim drives system is rare. Therefore, the capacitor sizing criteria for multiple slim drives system from the reliability aspect is studied in this section. For the case study, the multiple slim drives system specification is in accordance with parameters shown in Table I. The capacitance ranges from 20 μF to 60 μF and the relationship curve between capacitance and the resonant frequency of multiple slim drives system are shown in Fig. 29, where the capacitor sizing criteria in 10, 30 and 50 slim drives from the reliability aspect are investigated. It can be seen that: a) with the capacitance increases from 20 μF to 60 μF, the resonant frequency decreases from 700 Hz to 180 Hz; b) when 10 slim drives connected in parallel, the resonant frequency decreases from 700 Hz to 400 Hz. Especially at 27 μF, the resonant frequency is 600 Hz, which increase the gain for 600 Hz ripple; c) when 30 slim drives connected in parallel, the resonant frequency decreases from 400 Hz to 230 Hz. Especially at 30 μF, the resonant frequency is close to 300 Hz, which increase the gain for 300 Hz ripple; d) when 50 slim drives connected in parallel, the resonant frequency decreases from 310 Hz to 180 Hz, so that the larger capacitance values move the resonant frequency away from 300 Hz, which reduces the gain for 300 Hz ripple.

The estimated lifetime of DC-link capacitor in 10, 30 and 50 slim drives under soft grid condition are shown in Fig.

This article has been accepted for publication in a future issue of this journal, but has not been fully edited. Content may change prior to final publication. Citation information: DOI 10.1109/TPEL.2020.3003236, IEEE Transactions on Power Electronics

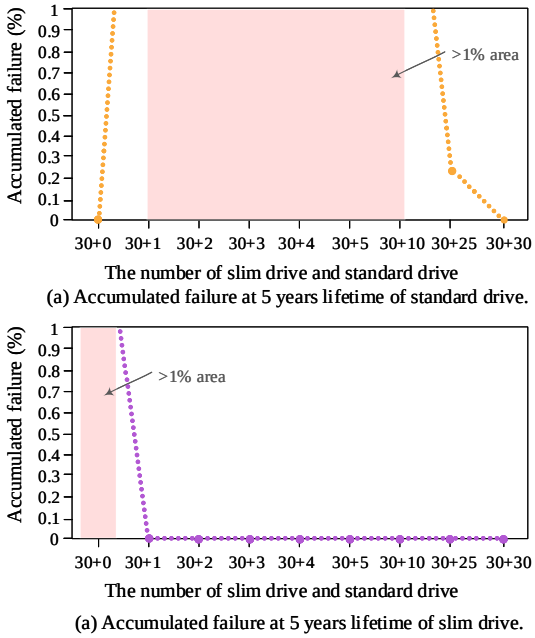

Fig. 28. Accumulated failure at 5 years lifetime of hybrid ASDs system under soft grid conditions. Keep the number of slim drive to 30 and increase the number of standard drive.

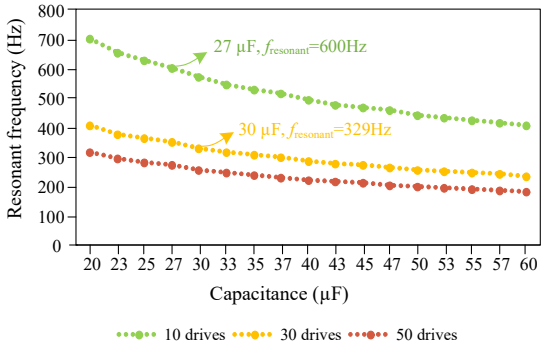

Fig. 29. Relationship between capacitance and resonant frequency of multiple slim drives under soft grid condition using parameters in Table I.

30 (a), (b) and (c), respectively. It shows that: a) when 10 slim drives connected in parallel, the B1 lifetime of DC-link capacitor with 27 μF is the shortest (i.e., 4.5 years); b) when 30 slim drives connected in parallel, the B1 lifetime of DC-link capacitor with 30 μF is the shortest (i.e., 4.3 years); c) when 50 slim drives connected in parallel, the B1 lifetime of DC-link capacitor with 20 μF is the shortest (i.e., 1.9 years). The relationship between DC-link capacitor B1 lifetime and capacitance under multiple slim drives are irregular, which is inconvenient for capacitor sizing, as a result, the relationship curve between DC-link capacitor B1 lifetime and capacitance under multiple slim drives are shown in Fig. 31, it shows that: a) when 10 slim drives connected in parallel, the B1 lifetime of DC-link capacitor with 27 μF is less than 5 years; b) when 30 slim drives connected in parallel, the B1 lifetime of DC-link capacitor with 30 μF to 33 μF is less than 5 years; c) when

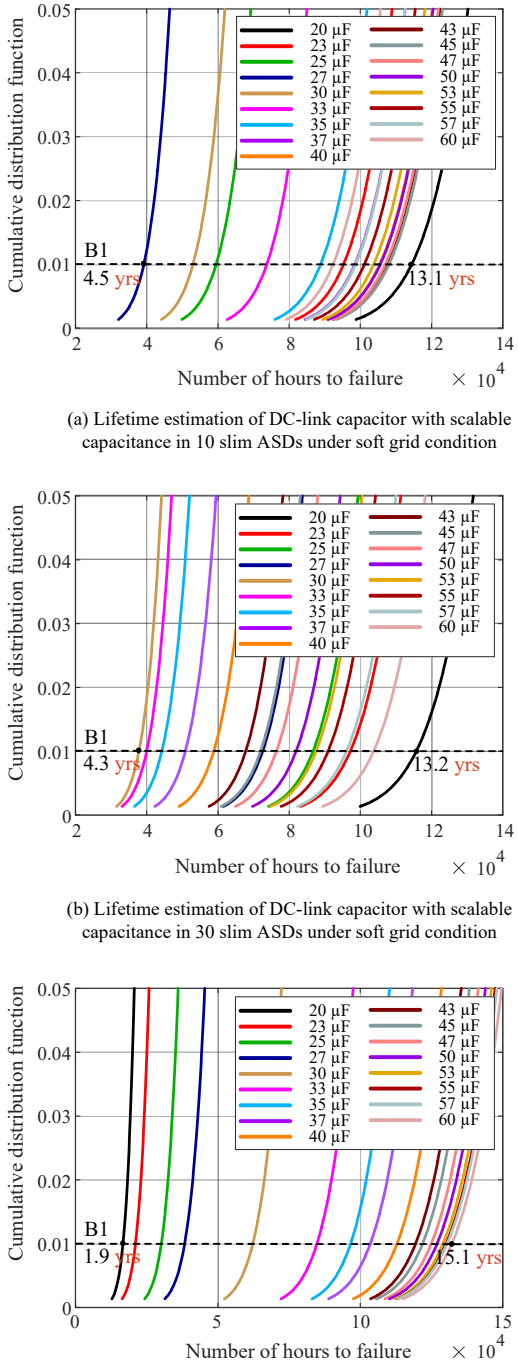

Fig. 30. Lifetime estimation of DC-link capacitor with scalable capacitance in multiple slim drives under soft grid condition (L_g= 130 μH).

50 slim drives connected in parallel, the B1 lifetime of DC-link capacitor with 20 μF to 27 μF is less than 5 years, and the larger the capacitance, the higher the reliability of DC-link capacitor.

VI. Conclusion

This paper investigates the lifetime of the DC-link capacitors in multi-drive systems. An analytical model to obtain

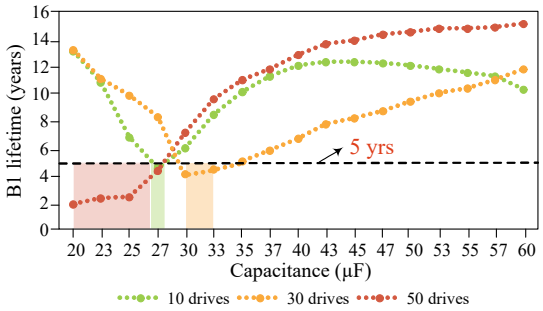

Fig. 31. The relationship between DC-link capacitor B1 lifetime and capacitance under multiple slim drives.

the DC-link continuous current in multiple standard and slim drives is provided, which makes the DC-link capacitor stress analysis away from simulation and becomes easy to modify and optimize. Based on the proposed analytical model and the lifetime prediction method, the relationship between the DC-link capacitor lifetime and the configurations of the multi-drive systems in terms of structures, numbers of drive and grid conditions is found. It quantifies that the impact of drive numbers and grid conditions, which should be considered in the concept and design phase of multiple ASDs. Based on the case study with the presented specification, following conclusions can be drawn :

1) In multiple standard drives, the B1 lifetime of DC-link capacitor extend with more drives connected in parallel at PCC, while in multiple slim drives, the shortest B1 lifetime of DC-link capacitor appears at 30 drives configurations;

2) The B1 lifetime of DC-link capacitor in 30 standard drives extend with larger grid impedance, while in 30 slim drives, the shortest B1 lifetime of DC-link capacitor appears at 130 μH and 150 μH grid impedance configurations;

3) The reliability of DC-link capacitor in slim drive is improved by adding standard drives to the ASDs system, however, the reliability of standard drive in hybrid ASDs system is worse, unless the standard drive reaches to a certain number.

4) From the reliability point of view, when multiple drives in soft grid and heavy load condition, the value of capacitor in 10 slim drives system grid should be selected other than 27 μF; for 30 slim drives system, the value of capacitor should be selected other than 30 μF to 33 μF; for 50 slim drives system, the value of capacitor should be selected larger than 27 μF in order to keep lifetime longer than 5 years in the studied case.

REFERENCES

[1] H. Wang, P. Davari, H. Wang, and D. Kumar, "Lifetime estimation of DC-Link capacitors in adjustable speed drives under grid voltage unbalances," *IEEE Trans. on Power Electron.*, vol. 34, no. 5, pp. 4064-4078, May. 2019.

[2] F. Zare, H. Soltani, D. Kumar and P. Davari, "Harmonic emissions of three-phase diode rectifiers in distribution networks," *IEEE Access.*, vol. 5, pp. 2819-2833, Mar. 2017.

[3] H. Wang and F. Blaabjerg, "Reliability of capacitors for DC-Link applications in power electronic converters—An Overview," *IEEE Trans. Ind. Appl.*, vol. 50, no. 5, pp. 3569-3578, Sep. 2014.

[4] H. Wang, M. Liserre and F. Blaabjerg, "Toward reliable power electronics—Challenges design tools and opportunities," *IEEE Ind. Electron. Mag.*, vol. 70, no. 2, pp. 17-26, Jun. 2013.

[5] S. Yang, A. Bryant, P. Mawby, D. Xiang, L. Ran and P. Tavner, "An industry-based survey of reliability in power electronic converters," *in Proc. IEEE ECCE*, pp. 3151-3157, 2009.

[6] M. A. Vogelsberger, T. Wiesinger and H. Ertl, "Life-cycle monitoring and voltage-managing unit for DC-Link electrolytic capacitors in PWM converters," *IEEE Trans. on Power Electron.*, vol. 26, no. 2, pp. 493-503, Feb. 2011.

[7] K. S. Rajashekara, V. Rajagopalan, A. Sevigny and J. Vithayathil, "DC-link filter design considerations in three-phase voltage source inverter-fed induction motor drive system," *IEEE Trans. Ind. Appl.*, vol. 23, no. 4, pp. 673-680, Jul. 1987.

[8] D. Kumar, P. Davari, F. Zare and F. Blaabjerg, "Analysis of three-phase rectifier systems with controlled dc-link current under unbalanced grids," *in Proc. IEEE APEC*, pp. 2179-2186, 2017.

[9] V. Dzhankhotov and J. Pyrhönen, "Passive *LC* filter design considerations for motor applications," *IEEE Ind. Electron. Mag.*, vol. 60, no. 10, pp. 4253-4259, Oct. 2013.

[10] H. Wang and H. Wang, "Performance evaluation of a two-terminal active Inductor in the DC-link filter of a three-phase diode bridge rectifier," *in Proc. IEEE APEC*, pp. 2844-2848, 2019.

[11] H. Wang, H. Wang, G. Zhu and F. Blaabjerg, "An overview of capacitive DC links - topology derivation and scalability analysis," *IEEE Trans. on Power Electron.*, vol. 43, no. 2, pp. 495-504, Mar. 2007.

[12] M. Hinkkanen and J. Luomi, "Induction motor drives equipped with diode rectifier and small DC-Link capacitance," *IEEE Trans. Ind. Electron.*, vol. 55, no. 1, pp. 312-320, Jan. 2008.

[13] H. M. Delpino and D. Kumar, "Line harmonics on systems using reduced DC-link capacitors," *in Proc. IEEE IECON*, pp. 961-966, 2013.

[14] M. F. Firuzi, A. Roosta and M. Gitizadeh, "Stability analysis and decentralized control of inverter-based ac microgrid," *Protection Control Mod. Power Syst.*, vol. 4, no. 6, pp. 1-24, Dec. 2019.

[15] H. Akagi, "Active harmonic filters," *Proc. IEEE*, vol. 93, no. 12, pp. 2128-2141, Dec. 2005.

[16] J. C. Das, "Passive filters - potentialities and limitations," *IEEE Trans. Ind. Electron.*, vol. 40, no. 1, pp. 232-241, Jan. 2004.

[17] H. Wen, W. Xiao, X. Wen and P. Armstrong, "Analysis and evaluation of dc-link capacitors for high-power-density electric vehicle drive systems," *IEEE Trans. Veh. Technol.*, vol. 61, no. 7, pp. 2950-2964, Sep. 2012.

[18] Y. Yang, K. Ma, H. Wang and F. Blaabjerg, "Instantaneous thermal modeling of the dc-link capacitor in photovoltaic systems," *in Proc. IEEE APEC*, pp. 2733-2739, 2015.

[19] H. Wang and H. Wang, "Benchmark of DC-link LC filters based on passive inductor and two-terminal active inductor," *in Proc. IEEE ICIT*, pp. 388-393, 2019.

[20] M. Chen, H. Wang, H. Wang, F. Blaabjerg, X. Wang and D. Pan, "Reliability assessment of hybrid capacitor bank using electrolytic- and film-capacitors in Three-Level Neutral-Point-Clamped Inverters," *in Proc. IEEE APEC*, pp. 2826-2832, 2019.

[21] B. K. Bose, "Power electronics and motor drives recent progress and perspective," *IEEE Trans. Ind. Electron.*, vol. 56, no. 2, pp. 581-588, Feb. 2009.

[22] H. Saren, O. Pyrhonen, K. Rauma and O. Laakkonen, "Overmodulation in voltage source inverter with small DC-link capacitor," *in Proc. IEEE PESC*, pp. 892-898, 2005.

[23] H. Wang, P. Davari, D. Kumar and F. Zare, "The impact of grid unbalances on the reliability of DC-link capacitors in a motor drive," *in Proc. IEEE ECCE*, pp. 4345-4350, 2017.

[24] H. Wang, P. Davari, H. Wang, and D. Kumar, "Lifetime benchmarking of two DC-link passive filtering configurations in adjustable speed drives," *in Proc. IEEE APEC*, pp. 228-233, 2018.

[25] F. Zare, "Harmonics issues of three-phase diode rectifiers with a small DC-link capacitor," *in Proc. IEEE PEMC*, pp. 912-917, 2014.

[26] M. Sakui, H. Fujita and M. Shioya, "A method for calculating harmonic currents of a three-phase bridge uncontrolled rectifier with DC filter," *IEEE Trans. Ind. Electron.*, vol. 36, no. 3, pp. 434-440, Aug. 1989.

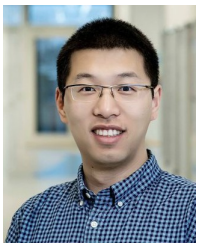

Haoran Wang (S'15-M'18) received the B.S. and M.S. degrees in control science and engineering from Wuhan University of Technology, Wuhan, China, in 2012 and 2015, respectively, and the Ph.D. degree in power electronics from Center of Reliable Power Electronics (CORPE), Aalborg University, Aalborg, Denmark, in 2018, where he is currently an Assistant Professor.

From Jul. 2013 to Sep. 2014, he was research assistant with the Department of Electrical Engineering, Tsinghua University, Beijing, China. He was a Visiting Scientist with the ETH Zurich, Switzerland, from Dec. 2017 to Apr. 2018. His research interests include capacitors in power electronics, reliability of power electronic systems, and multi-objective life-cycle performance optimization of power electronic systems.

Shili Huang (S'20) received the B.S. degree in electrical engineering from the Hubei University of Technology, Wuhan, China, in 2017. She is currently working toward the master's degree in electrical engineering with the Wuhan University of Technology, Wuhan.

Her research interests include capacitors in power electronics, reliability of power electronic systems and DC-link capacitor.

Dinesh Kumar (S'08-M'12-SM'20) received Master of Technology (M. Tech) in power system engineering from Indian Institute of Technology (IIT), Roorkee, India, in 2004, and Ph.D. degree in power electronics from the University of Nottingham, U.K., in 2010. From 2004-2005, he served as a Lecturer in Electrical Engineering Department at National Institute of Technology, Kurukshetra, India. In 2006, he joined Technical University Chemnitz, Germany as a Research Fellow in Power Electronics. From 2006 to 2010, he investigated and developed matrix converter based multidrive system for aerospace applications. Since 2011, he is with the Danfoss Drives A/S, Denmark, where he is involved in many research and industrial projects. He is a member of the IEC standardization Working Group in TC77A and SyC LVDC committee. His current research interests include motor drive, harmonic analysis and mitigation techniques, power quality and electromagnetic interference in power electronics. He is the Editor-in-Chief of International Journal of Power Electronics and the Associate Editor of IEEE Transaction on Industry Applications and IEEE Access Journal.

Qian Wang (S'15-M'18) was born in Hubei Province, China in 1990. She received her Bachelor degree of Electrical Engineering from Wuhan University of Technology in 2012. In 2015, she obtained Master degree of High Voltage Engineering in Huazhong University of Science and Technology. She got her PhD in High Voltage Engineering from Department of Energy Technology, Aalborg University, Denmark in 2018. Now, she is an Assistant Professor in Aalborg University.

Her field of interests are electrical design / testing of innovative, composite-based transmission towers and insulation in modern power electronic components.

Xiangtian Deng (M'15) received the B.E. degree in electrical engineering from CTGU(China Three Gorges University), Yichang, China, in 2005 and the Ph.D. in electrical engineering from Wuhan University, Wuhan, China, in 2015.

He has been a faculty member with Wuhan university of technology since 2015, and is currently working as an Associate Professor with School of Automation, Wuhan, China. His research interest includes the control and protection of DC microgrid, active capacitor.

Guorong Zhu (M'09-SM'11) was born in Hunan, China. She received the Ph.D. degree in electrical engineering from the Huazhong University of Science and Technology, Wuhan, China, in 2009.

From 2002 to 2005, she was a Lecturer with the School of Electrical Engineering, Wuhan University of Science and Technology, Wuhan. From 2009 to 2011, she was a Research Assistant/Research Associate with the Department of Electronic and Information Engineering, The Hong Kong Polytechnic University, Hong Kong. From 2016 to 2017, she was a Visiting Scholar with the Department of Energy Technology, Aalborg University, Aalborg, Denmark. She is currently an Associate Professor with the School of Automation, Wuhan University of Technology, Wuhan. Her research interests include power electronics equipment reliability, battery energy storage technology, and wireless power transfer technology.

Huai Wang (M'12-SM'17) received the B.E. degree in electrical engineering, from Huazhong University of Science and Technology, Wuhan, China, in 2007 and the Ph.D. degree in power electronics, from the City University of Hong Kong, Hong Kong, in 2012.

He is currently a Professor at the Center of Reliable Power Electronics (CORPE), Aalborg University, Aalborg, Denmark. He was a Visiting Scientist with the ETH Zurich, Switzerland, from Aug. to Sep. 2014, and with the Massachusetts Institute of Technology (MIT), USA, from Sep. to Nov. 2013. He was with the ABB Corporate Research Center, Switzerland, in 2009. His research addresses the fundamental challenges in modelling and validation of power electronic component failure mechanisms, and application issues in system-level predictability, condition monitoring, circuit architecture, and robustness design.

Dr. Wang received the Richard M. Bass Outstanding Young Power Electronics Engineer Award from the IEEE Power Electronics Society in 2016, and the Green Talents Award from the German Federal Ministry of Education and Research in 2014. He is currently the Award Chair of the Technical Committee of the High Performance and Emerging Technologies, IEEE Power Electronics Society, and the Chair of IEEE PELS/IAS/IE Chapter in Denmark. He serves as an Associate Editor of IET POWER ELECTRONICS, IEEE JOURNAL OF EMERGING AND SELECTED TOPICS IN POWER ELECTRONICS, and IEEE TRANSACTIONS ON POWER ELECTRONICS.